Enhancing cell seeding and osteogenesis of MSCs on 3D printed scaffolds through injectable BMP2 immobilized ECM-Mimetic gel

*Farahnaz Fahimipour [a,f,1], Erfan Dashtimoghadam [a,1],
Mohammad Mahdi Hasani-Sadrabadi [b,c], Jessica Vargas [a],
Daryoosh Vashaee [d], Douglas C. Lobner [e], Tahereh S. Jafarzadeh Kashi [f],
Behnam Ghasemzadeh [g], Lobat Tayebi [a,*]*

[a] *Marquette University School of Dentistry, Milwaukee, WI 53233, USA*
[b] *Parker H. Petit Institute for Bioengineering and Bioscience, G.W. Woodruff School of Mechanical Engineering, Georgia Institute of Technology, Atlanta, GA 30332, USA*
[c] *Weintraub Center for Reconstructive Biotechnology, Division of Advanced Prothodontics, School of Dentistry, University of California, Los Angeles, CA 90095, USA*
[d] *Electrical and Computer Engineering Department, North Carolina State University, Raleigh, NC 27606, USA*
[e] *Department of Biomedical Sciences, Marquette University, Milwaukee, WI 53233, USA*
[f] *Dental Biomaterials Department, School of Dentistry, Tehran University of Medical Sciences, Tehran, Iran*
[g] *Department of Biomedical Sciences, Integrative Neuroscience Research Center, Marquette University, Milwaukee, WI 53201, USA*

ARTICLE INFO

ABSTRACT

Objective. Design of bioactive scaffolds with osteogenic capacity is a central challenge in cell-based patient-specific bone tissue engineering. Efficient and spatially uniform seeding of (stem) cells onto such constructs is vital to attain functional tissues. Herein we developed heparin functionalized collagen gels supported by 3D printed bioceramic scaffolds, as bone extracellular matrix (ECM)-mimetic matrices. These matrices were designed to enhance cell seeding efficiency of mesenchymal stem cells (MSCs) as well as improve their osteogenic differentiation through immobilized bone morphogenic protein 2 (BMP2) to be used for personalized bone regeneration.

Methods. A 3D gel based on heparin-conjugated collagen matrix capable of immobilizing recombinant human bone morphogenic protein 2 (BMP2) was synthesized. Isolated dental pulp Mesenchymal stem cells (MSCs) were then encapsulated into the bone ECM microenvironment to efficiently and uniformly seed a bioactive ceramic-based scaffold fabricated using additive manufacturing technique. The designed 3D cell-laden constructs were comprehensively investigated trough *in vitro* assays and *in vivo* study.

Results. In-depth rheological characterizations of heparin-conjugated collagen gel revealed that elasticity of the matrix is significantly improved compared with freely incorporated heparin. Investigation of the MSCs laden collagen-heparin hydrogels revealed their capability to provide spatiotemporal bioavailability of BMP2 while suppressing the matrix contraction over time. The *in vivo* histology and real-time polymerase chain reaction (qPCR) analysis showed that the designed construct supported the osteogenic differentiation of MSCs and induced the ectopic bone formation in rat model.

Significance. The presented hybrid constructs combine bone ECM chemical cues with mechanical function providing an ideal 3D microenvironment for patient-specific bone tissue engineering and cell therapy applications. The implemented methodology in design of ECM-mimetic 3D matrix capable of immobilizing BMP2 to improve seeding efficiency of customized scaffolds can be exploited for other bioactive molecules.

1. Introduction

Regeneration of critical-sized bone defects needs clinical interventions in most cases in order to restore, maintain or improve the bone function [1–3]. Bone tissue engineering (BTE) techniques are introduced to eliminate the pitfalls of bone grafts, which relies on delivery or recruitment of cells and bioactive agents through three dimensional (3D) scaffolds. Over the past years, 3D printing techniques have shown great potential to fabricate customized scaffolds with complex geometries and controlled pore structure [4–7]

An ideal scaffold should not only support the complex geometries of bone defects to guide the bone tissue regeneration, but also provide a porous microenvironment to recruit biologics and regulate cellular growth and differentiation [8,9]. However, generation of cell-seeded implantable 3D scaffold is still remained problematic due to the low cell seeding efficiency and deficient cellular distribution [10]. To enhance cell delivery to the defect, encapsulation of regenerative cells into the external matrix has been proposed. Biomimetic hydrogels have shown promising capabilities to meet the demands for cell delivery, local, and sustained release of growth factors [11,12]. In addition to the capability of hydrogels to provide cells anchorage, chemical cues, proper viscoelasticity and stiffness are essential for viability and fate of the encapsulated cells [13–16].
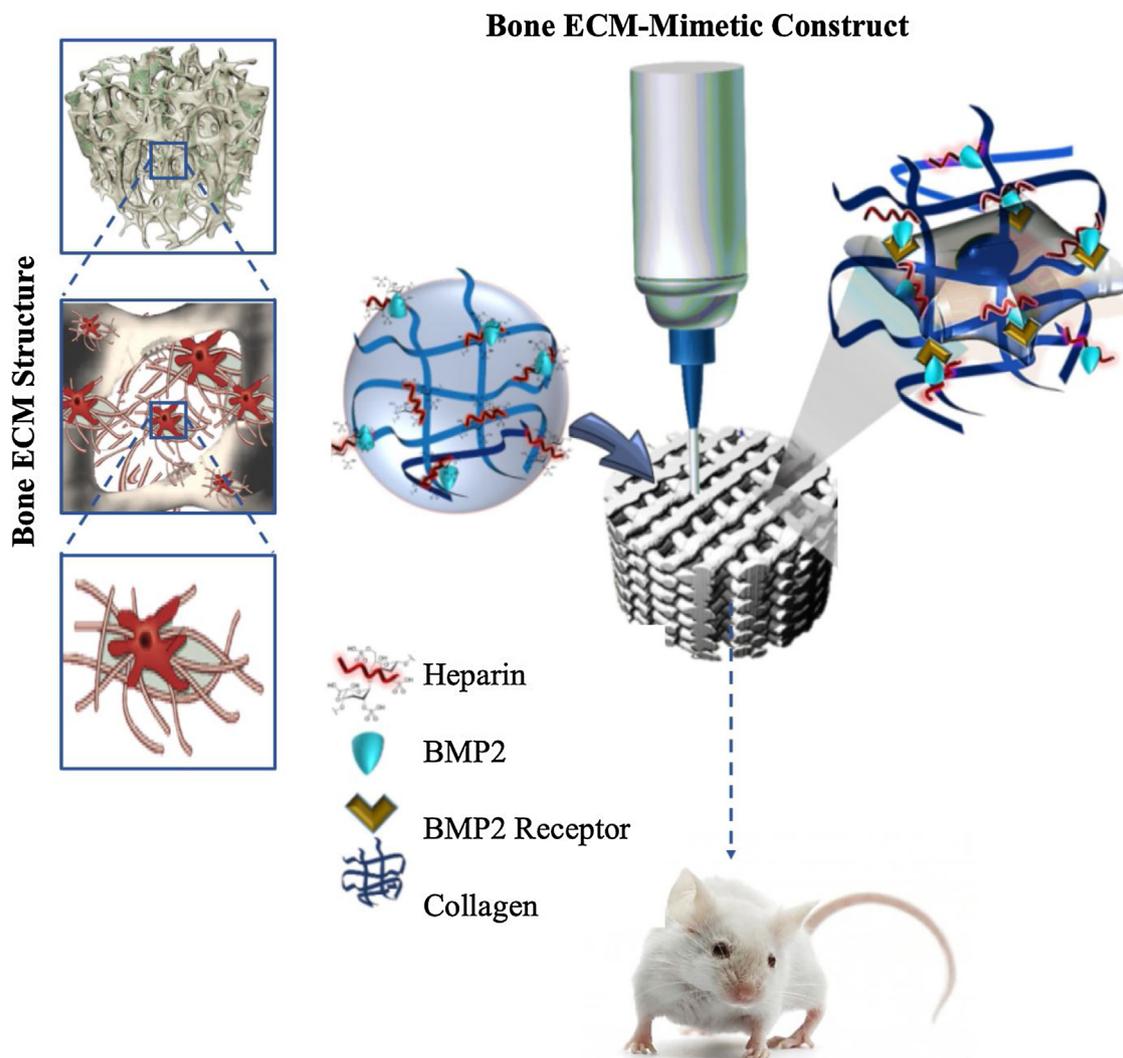
Collagen as the main component of the native ECM has been widely used as an appropriate biomaterial for cell encapsulation due to its favorable biocompatibility, degradation, and tissue regeneration potential properties [4,17]. Encapsulation of MSCs within injectable collagen has demonstrated not only preservation of cells' differentiation potential, but also cell viability upon *in vivo* implantation [18]. Despite favorable characteristics of collagen hydrogels, the shortcomings of gel-like collagen matrices including matrix contraction and low mechanical properties impede their application for hard tissue engineering [19].

There has been a great deal of interest in using mesenchymal stem cells (MSCs) for bone regeneration owing to their ability to provide osteoinductive bone factors and differentiation to osteoblasts *in vitro* and *in vivo* [20,21]. It has been reported that engineering of bone tissue with enriched delivery of MSCs is a promising approach to improve the regeneration [22].

In this view, forming MSCs laden collagen matrices within supportive mineral-based 3D printed scaffolds promises an ideal biomimetic approach through harvesting the advantages of hydrogel-mediated efficient cell delivery and mechanically robust scaffold. Several evidences have shown that MSCs engineered with bone morphogenetic protein 2 (BMP2) more effectively induced bone formation than MSC implantation alone in both ectopic and orthotopic sites. Bone morphogenetic protein2 (BMP2) has been confirmed to promote osteogenic differentiation of mesenchymal stem cells (MSCs) as well as ectopic bone formation [23,24]. In native ECM, BMP2 exist in soluble as well as in matrix-bound forms [25,26]. Although rhBMP2 has successfully been administered clinically through collagen-based carriers to stimulate bone regeneration, a high dose of rhBMP2 is required, likely due to its short half-life *in vivo* [27,28]. Several studies demonstrated that bound growth factor to the ECM conveys signaling by prolonged activation of receptors and differential phosphorylation [24]. The major advantage of growth factor immobilization is improved efficiency, *i.e.*, a small amount, and controlled presentation of the molecule [29]. The distinct biocharacteristics of glycosaminogycans (GAGs) like heparan sulfate, make them valuable biomolecules for binding and modulation of growth factors, and ECM proteins [30–32]. It has been reported that incorporation of GAGs into different hydrogel matrices is potentially beneficial to achieve immobilization and sustained bioavailability of rhBMP2 [33,34].

Herein a reinforced hybrid construct has been developed to mimic natural bone ECM. The heterophasic constructs consisted of a 3D collagen-based matrix encapsulating cells, which is mechanically supported by a reinforced ceramic scaffold (Scheme 1). The ceramic scaffold, as the mineral phase of the constructs, was composed of β-TCP nanoparticles and fabricated using the 3D printing technique. The 3D

Bone ECM-Mimetic Construct

Heparin

BMP2

BMP2 Receptor

Collagen

Ectopic Bone Formation In Rat Model

Bone ECM Structure

Scheme 1 – The schematic representation of the developed approach to enhance in situ seeding and osteogenesis of MSCs on 3D printed scaffold through injectable BMP2 immobilized Collagen Heparin gel.

microenvironment for cellular activity was synthesized based on heparin immobilized collagen gel-like matrices with capability of providing sustained bioavailability of rhBMP2. The collagen matrix was chemically functionalized with heparin to not only provide binding of rhBMP2, but also control the contraction of the cell-laden matrix. Mesenchymal stem cells were encapsulated into the bone ECM-mimetic collagen-based matrices.

2. Methods and materials

2.1. Design and characterization of ECM mimetic collagen-heparin (Col-Hep) matrix

2.1.1. Synthesis of heparin conjugated collagen
The collagen matrix was modified through chemical functionalization with heparin (Hep) in order to achieve binding domains for the growth factor, which is described below. The

carboxyl groups of Hep were activated *via* carbodiimide chemistry prior to reaction with collagen chains. In brief, 5 mg heparin sodium salt (Alfa Aesar) was activated with 10 mg 1-(3-dimethylaminopropyl)-3-ethylcarbodiimide hydrochloride (EDC, TCI Chemicals) and 6 mg N-hydroxysuccinimide (NHS, Alfa Aesar) in 2.5 ml 0.05 M 2-[N-Morpholino] ethanesulfonic acid (MES, MP Biomedicals) solution for 10 min at 37 °C. The activated heparin solution was dialyzed through a dialysis membrane (Spectra/Por®, MWCO: 3.5–5 kD) with 500 ml water for one day to remove excess EDC/NHS. Afterward, the activated heparin solution was precipitated, and then kept overnight at −80 °C. The samples were freeze-dried at 1 Pa and −52 °C for 24 h followed by overnight secondary drying at room temperature and 1 Pa. The free heparin and activated heparin solution were added at various concentrations (50 and 100 µg ml^{-1}) to the collagen solution (Bovine collagen type I, Advanced BioMatrix). The ECM mimetic collagen-heparin (Col-Hep) matrices were prepared by mixing the collagen solu-

tion at 4 °C with 10× concentrated Dulbecco's Modified Eagle Medium (DMEM) and Hank's Balanced Salt Solution (HBSS) to achieve 2.5 mg ml⁻¹ for collagen content and then neutralized to pH 7.4 using 1N NaOH. After being well mixed, the collagen-based solutions were incubated at 37 °C for 30 min for gelification.

The conjugation efficiency of heparin onto collagen matrices was analysed using the toluidine blue assay. The conjugation efficiency was carried out at room temperature with distilled water as the release medium under gentle stirring. 2 ml of released solution was thoroughly mixed with 3 ml of toluidine blue solution (2 mg of toluidine blue, 230 mg NaCl in 250 ml 0.01 M hydrochloric acid). 3 ml of *n*-hexane was then added, and the mixture was shaken well in order to extract the heparin into the organic layer. Finally, the absorbance of the aqueous phase was measured at different time intervals using a spectrophotometer (Thermo Scientific™ Evolution™ 220 UV–vis Spectrophotometer) at 631 nm [35].

2.1.2. Characterization of col-hep matrices

2.1.2.1. *Physicochemical characterization of col-hep matrices.* The microstructural changes in collagen matrices after functionalization with activated heparin chains were examined by scanning electron microscopy (SEM; JEOL JSM-6510LV). The denaturation behavior of collagen chains in freeze-dried Col-Hep sample was investigated by differential scanning calorimetry method (DSC; NETZSCH DSC 404 F1 Pegasus®), and compared with that of for pristine collagen. DSC measurements were carried out on 5 mg sample in aluminum crucibles with pierced lid under 20 ml min⁻¹ ultra-pure argon flow. In order to ensure the samples were fully dried, the crucibles were heated to 130 °C, incubated for 30 min, and then heated to 250 °C at a 10 °C min⁻¹ heating rate. The chemical structure of Col-Hep matrices was examined using the Fourier-transform infrared spectroscopy method (FT-IR; Nicolet™ iS5, iD5 Diamond Attenuated total reflection, Thermo Scientific™) [36].

2.1.2.2. *Rheological measurements of collagen-based matrices.* Oscillatory shear measurements were performed by means of a Malvern Kinexus pro + rheometer using a cone-and-plate geometry (diameter: 40 mm, cone angle: 4°). After loading samples, the cone and plate were covered to avoid sample dehydration. Strain amplitude of 1% was applied to minimize the network perturbation during measurements. Prior to temperature sweep measurements at different frequencies, the strain amplitude sweep measurement was performed to ensure the measurements were conducted in the linear viscoelastic regime and the viscoelastic features (dynamic storage modulus G' and loss modulus G'') are independent of the strain amplitude [13,37]. The oscillatory frequency sweep measurements were carried out over the angular frequency (ω) interval of 0.1–10 rad/s, while the temperature was increased with a heating rate of 1 K min⁻¹. The time sweep measurements were performed at 37 °C, strain amplitude of 1%, and frequency of 1 rad s⁻¹ for 150 min.

2.1.3. Matrix contraction assay
The collagen-based gel-like matrices (Col and Col-Hep) were prepared as described above. Subsequently, the resultant solu-

tion was mixed with 1×10^6 MC3T3. The obtained constructs were kept at room temperature for 30 min, and then placed in an incubator under a humidified atmosphere of 5% CO₂ in air at 37 °C. The contraction of collagen-based gel-like matrices was measured in triplicate. The matrix contraction was measured at various time intervals of 12, 24, 48, and 72 h [38].

2.1.4. Immobilization of rhBMP2 and in vitro release profiles
Five μg rhBMP2 (Cell Applications, Inc) was mixed with the collagen-based solutions (Col and Col-Hep) prior to gelification according to the procedure described above. Col and Col-Hep matrices were then incubated in phosphate buffered saline (PBS; 120 mM NaCl, 2.7 mM KCl, 10 mM phosphate buffer salts), and after 4 h, 100 μl samples of the supernatant were collected to measure the rhBMP2 washout. The samples withdrawn for analysis were then replaced with the same volume of fresh medium. The *in vitro* release of rhBMP2 from Col and Col-Hep matrices was evaluated in PBS buffer solution according to a similar procedure at scheduled time intervals of 1, 3, 7, 14 and 21 days. The collected samples were centrifuged at 5000 rpm at room temperature and the supernatant was analyzed for rhBMP2 content *via* ELISA kit (Cell Applications, Inc.). The concentration of rhBMP2 was calculated in ng ml⁻¹ of the solution.

2.1.5. BMP2 bioactivity assay
The viability of MC3T3 cells [39] encapsulated into collagen-based matrices were evaluated using LIVE/DEAD cell viability assays (Thermo Fisher Scientific) at days 3 and 7. In brief, cell-laden matrices were washed with sterile PBS three times for 10 min and then incubated for 1 h with 4 mM calcein-AM and 4 mM ethidium homodimer in PBS at room temperature. After incubation, matrices were washed again for fluorescence microscopy (EVOS FL Auto Cell Imaging System, Thermo Fisher Scientific). The bioactivity of BMP2 was assessed utilizing an Alkaline Phosphatase (APase) Assay Kit based on a colorimetric assay kit (Abcam, USA). The APase activity of MC3T3 cells when encapsulated into the Col-Hep, Col/rhBMP2 and Col-Hep-rhBMP2 matrices was assessed after 7 and 14 days according to the manufactures protocol. In brief, the cells were digested, collected, and lysed. Subsequently, 30 μl samples from lysate was added to a 96-well plate with 50 μl of the assay buffer and 50 μl of pNPP. The samples were covered and incubated at room temperature for 1 h. Subsequently, 20 μl of stop solution (3 N NaOH) was added to the wells, and the absorbance of p-nitrophenol was measured at 405 nm using a microplate spectrophotometer (Synergy™ HTX Multi-Mode Microplate Reader, Bio-Tek Instrument). Cell lysates were also analyzed for protein content using a micro-BCA Assay kit (Pierce), and ALP activity was normalized to the total protein content, which was measured using Pierce BCA protein assay kit (Thermo Fisher Scientific). Alkaline phosphatase activity is expressed in arbitrary units. The results represent the mean values of three individual experiments and each in quadruplicate.

Table 1 – 3D printing parameters.

Ceramic paste temperature	20 °C
Platform temperature	RT
Pressure	1.2 bar
Speed	3 mm/s
Distance between strands	600–800 μm
Slice width	150 μm

2.2. Fabrication and characterization of 3D printed β-TCP scaffolds

2.2.1. 3D printing of β-TCP scaffolds

The ceramic based paste ink formulation was composed of 75 wt.% beta-tricalcium phosphate powder (β-TCP, Sigma), 0.35 wt.% carboxymethylcellulose (CMC, Alfa Aesar) as the binder, 2.5 wt% sodium tripolyphospahte (TPP, Alfa Aesar) as the viscosity modifier, and 5 wt.% colloidal silica nanoparticles (cSiO$_2$, LUDOX®, Sigma) as the high temperature binder. The paste components were mixed in aqueous medium using a planetary centrifugal mixer (THINKY Mixer, ARE-310). Carboxymethyl cellulose (CMC) is an organic binder that have been widely used in ceramic shaping to enhance the performance of bodies during process and applications. It has been reported that CMC improve the mechanical strength of dry bodies and completely burn out during firing. Prior to printing, the temperature of the paste reservoir was set to 20 °C for 10 min. The formulated pastes were then injected out of the nozzle by air flow to layer-by-layer fabricate disk-shaped (7 mm diameter and 2 mm thickness) porous scaffolds based on pre-designed models with CAD/CAM software. Scaffolds were consisted of 10 printed layers in total. The 3D printing process was performed at 3 mm/s dispensing speed, optimal pressure of 1.2 bar, and a plotting needle (Nordson, USA) with an inner diameter of 400 μ m (Table 1). The scaffolds were printed with 600–800 μm distance between strands and a 90° shift between layers. Scaffolds were air dried at room temperature overnight, sintered in a furnace (KSL-1700X-S-UL, MTI) at 600 °C for 1 h, and then at 1100 °C for 4 h.

2.2.2. Characterization of β-TCP scaffolds

The 3D printed scaffolds were characterized by their microstructure (pore size and thickness of strands) using a 3D Laser Measuring Microscope (Olympus LEXT OLS 4000, Japan). The mechanical properties of β-TCP-based scaffolds were measured according to ASTM standards using in compression mode using a universal testing machine (AGS-X series, 5 kN load cell, Shimadzu, Japan) at a speed of 1 mm min^{-1}. The porosity of scaffold was quantified using previously reported solvent displacement method [20]. For this purpose, the weight of scaffolds was measured in dry condition and immersed in 10 ml ethanol, then the porosity was analysed using the following equation:

$$Porosity = \frac{(W_w - W_d) \times 100\%}{\rho \times \pi \mathcal{R}^2 T}$$

In which ρ is the solvent density, W$_d$ and W$_w$ are the weight of scaffold in dry and wet condition, and R, T are the radius and thickness of scaffolds, respectively.

At least three sintered cylindrical samples (5 mm diameter, 10 mm height) were compressed until they cracked. Elastic moduli were derived from the initial linear region of the stress-strain curves.

2.2.3. Dental pulp mesenchymal stem cells seeding strategies

Dental pulp mesenchymal stem cells (MSCs) were isolated as described elsewhere [4]. In brief, normal impacted third molars were first washed in PBS containing 100 U ml^{-1} penicillin and 100 mg ml^{-1} streptomycin (GIBCO, Invitrogen Corporation). After cutting the crown, the pulp tissue was removed. In the next step, the pulp tissue was digested using a solution comprising 3 mg ml^{-1} collagenases type I (Alfa Aesar) and 4 mg ml^{-1} dispase (Sigma) in Hank's Balanced Salt Solution (HBSS, Sigma) for 1 h at 37 °C with regular agitation. The digested mixture was added to alpha-minimal essential medium (α-MEM, Sigma) supplemented with 15% fetal bovine serum (FBS, Sigma), seeded in culture dishes and incubated in 5% CO$_2$ at 37 °C. The expression of cell-surface markers of dental pulp cells was determined by the fluorescence activated cell sorting (FACS) technique (Attune® Acoustic Focusing Cytometer, Thermo Fisher Scientific). In order to verify the osteogenic capability of the cells, the alizarin red assay was carried out. In brief, the extracted cells at passage 3 were cultured on tissue culture polystyrene for 3 weeks in an osteogenic medium, consisting of αMEM supplemented with 10% FBS, 50 μg/ml ascorbic acid, 10 mM β-glycerophosphate and 10 nM dexamethasone. Then, the samples were fixed, washed and stained with alizarin solution (Alfa Aesar).

Prior to in vitro cell culture studies, the disk-shaped 3D printed scaffolds were disinfected using 70 wt.% aqueous ethanol solution. The disinfection process included three times immersion in 70% ethanol for 15 min followed by rinsing with PBS cycles and air drying. Afterward, 1×10^6 cells were seeded on the scaffold through two approaches. (1) MSCs were directly seeded onto the scaffolds which were placed in a non-adherent 12 well-plate and then submerged in culture medium. The medium was changed every other day; (2) MSCs were loaded through cell-laden thermogels and then added to the construct on the ice and then the constructs were incubated in 37C to solidify the gel.

For PrestoBlue® cell vitality, after the incubation period, 10% Presto blue was added to the scaffold-cell complexes. Fluorescence measurements (Ex: 560 nm and Em: 590 nm) were determined by a spectrophotometric plate reader (Synergy HTX, BioTEK). The alkaline phosphatase (APase) activity was measured based on a colorimetric assay kit using p-nitrophenyl phosphate (pNPP) as a phosphatase substrate (Abcam, USA). Triplicate samples were analyzed for this experiment. PrestoBlue® cell vitality assay (Thermo Fisher Scientific) and APase Activity (Abcam, USA) was performed according to the manufacturer's instructions after 3, 7 and 14 days of cell culture on scaffolds.

2.3. Characterization of reinforced collagen-based matrices

2.3.1. Cell seeding efficiency and cell adhesion

Cell seeding efficiency was analysed as described elsewhere [40]. In brief, the cells were loaded onto the scaffolds which were placed in a non-adherent 6 wells plate and incubated

for 12 h in 5% CO_2 at 37 °C. Then, the scaffolds were removed and the number of remaining cells in the wells was measured using a counting chamber method. Considering the number of loaded cells, the seeding efficiency was calculated using the following equation,

$$Cell\ seeding\ efficiency\ (\%)$$
$$= \frac{(cells\ loaded\ on\ scaffold - residual\ cells\ in\ wells)}{cells\ loaded\ on\ the\ scaffold} \times 100$$

The reinforced cell-laden collagen-based gel-like matrices, βTCP/Col, βTCP/Col-Hep and βTCP/Col-Hep-BMP2 constructs, were characterized using scanning electron microscopy. In brief, the scaffolds were removed from the culture medium after predetermined incubation times, washed in PBS, fixed with Karnovsky's Fixative, and then dehydrated in gradient aqueous ethanol solutions of 50, 60, 70, 80, 90 and 100%. Samples were gold sputter coated using a GSL-1100X-SPC12 Compact Plasma Sputtering Coater instrument, and then scanned by the scanning electron microscope (JEOL JSM-6510LV).

2.3.2. Cell proliferation

In order to examine the cell proliferation in βTCP/Col, βTCP/Col-Hep and βTCP/Col-Hep-rhBMP2 constructs aDNA quantification assay was conducted at 3, 7, 14 and 21 days. The DNA quantification was carried out by means of the Quant-iT™ PicoGreen® dsDNA Assay Kit (Thermo Fisher Scientific) following the manufacturer's protocol. In Brief, constructs were first digested in 1 ml of 4 M guanidine hydrochloride buffer (pH = 7.5). Afterward, 50 μl of samples or DNA standards were incubated with 150 μl of 1 × PicoGreen reagents. Finally, fluorescence measurements (Ex 480 nm/Em 520 nm) were performed by a spectrophotometric plate reader (Synergy™ HTX Multi-Mode Microplate Reader, Bio-Tek Instrument).

2.3.3. Cell differentiation

APase activity, immunocytochemistry, and Quantitative real-time polymerase chain reaction(qPCR) were performed to assess the MSCs differentiation. The Alkaline Phosphatase Assay Kit (Abcam) was used according to the manufactures protocol.

For osteocalcin (OCN) immunocytochemistry, the samples were first fixed with 4% paraformaldehyde and then permeabilized. Afterward, the samples were incubated in primary osteocalcin antibody (1:100) and subsequently in anti-rabbit antibody Alexa Fluor 647 (Abcam). The cells nuclei were then stained using DAPI.

In order to perform qPCR assay, the scaffolds (n = 6) were collected at days 7 and 14, then pulverized. Total RNA was extracted using Trizol reagent (Invitrogen) following the instructions provided. RNA (1 μg) was used to reverse transcribed into complementary DNA (cDNA) (Invitrogen). For the polymerase chain reaction (PCR), aliquots of synthesized cDNA were added to SYBR® Green PCR Master Mix (Applied Biosystems, USA) and cycled on a DNA thermal cycler. Primers for PCR were as follows: 1) Alkaline phosphatase (ALP) fwd 5′-ACGTGGCTAAGAATGTCATC-3′, rev: 5′-CTGGTAGGCGATGTCCTTA-3′, 2) Osteocalcin (OCN) fwd: 5′-

CATGAGAGCCCTCACA-3′ rev: 5′-AGAGCGACACCCTAGAC-3′, 3) Runt-related transcription factor 2 (RUNX II) fwd: 5′-TCTTCACAAATCCTCCCC-3′ rev: 5′-TGGATTAAAAGGACTTGG-3′, 4) β-ACTIN fwd: 5′-AGCCATGTACGTTGCTA-3′ rev: 5′-AGTCCGCCTAGAAGCA-3′. All experiments were performed in triplicate.

2.4. Subcutaneous implantation of constructs

For this study, Male Fischer 344 rats with age: 7–8-week-old were used in our animal study based on a protocol approved by the Institutional Animal Care and Use Committee (IACUC) of Marquette University. The rats were housed in a temperature and humidity-controlled environment on a 12/12 h light/dark cycle, with food and water made available ad libitum. 5×10^6 MSCs were encapsulated in heparin conjugated collagen hydrogels, heparin conjugated collagen hydrogels immobilized with 25 μg/ml rhBMP2 or collagen hydrogels containing 25 μg/ml rhBMP2. The disk-like MSC-scaffolds with 7 (diameter) × 2 (thickness) mm dimension were subcutaneously implanted into the dorsum of animals. The constructs without rhBMP2 were used as negative controls. Five animals (n = 5) in each group were used with two transplants in each. The implanted MSCs were harvested six weeks post-surgery. For histological tissue processing, harvested samples were fixed in 4% para formaldehyde (PFA) for 24 h and decalcified in 10% EDTA at 4 °C for 6 weeks. Samples were then dehydrated in ethanol and embedded in paraffin. Sections (5 μm) were cut using a microtome. The slides were then deparaffinized and rehydrated in a graded ethanol series (100%, 90%, and 70% ethanol, 5 min each; dH_2O for 10 min) before being stained with hematoxylin and eosin (H & E). In order to perform qPCR assay, tissue was collected after 6 weeks, then pulverized (n = 4). The total RNA was extracted using Trizol reagent (Invitrogen), following the instructions provided. RNA (1 μg) was used to reverse transcribed into complementary DNA (cDNA) (Invitrogen). For the polymerase chain reaction (PCR), aliquots of synthesized cDNA were added to with SYBR® Green PCR Master Mix (Applied Biosystems, USA) and cycled on a DNA thermal cycler. All experiments were performed in triplicate.

2.5. Statistical analysis

All data were expressed as mean ± standard deviation (Mean ± SD). The significance difference was calculated by one-way ANOVA complemented by Tukey's multiple comparisons test. P-values < 0.05 were considered to be statistically significant.

3. Results

3.1. ECM mimetic heparin conjugated collagen matrices

The structural stability of heparin in collagen matrix incorporated either using preactivated by carbodiimide reaction or simple mixing was measured based on Hep release over 7 h at physiological pH (7.4). As shown in Fig. 1A, 51.9 ± 4.1% of the 50 μg ml⁻¹ simply mixed Hep was released after
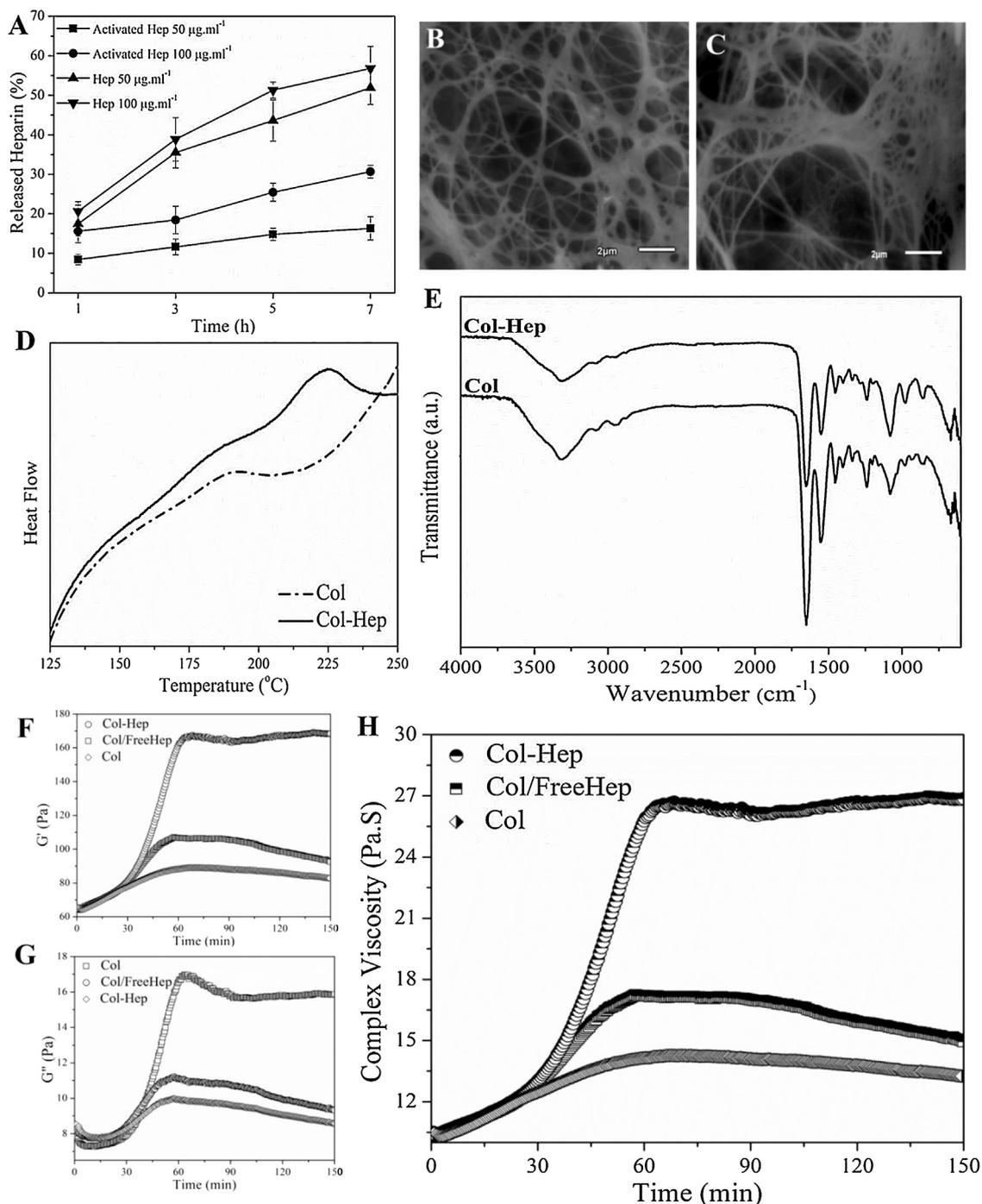
Fig. 1 – (A) The release pattern of heparin incorporated in different forms (free and activated at 50 or 100 ng ml^{-1}) from various collagen-based matrices (Col and Col-Hep) at physiological condition (pH 7.4, 37 °C). Scanning electron micrograph of (B) Col, and (C) Col-Hep matrix (scale bar is 100 μm). (D) Differential scanning calorimetry thermograms of freeze-dried Col and Col-Hep matrices. (E) Fourier transform infrared spectra of Col, and Col-Hep matrices. (F) The storage modulus (G′), (G) loss modulus (G″), and (H) complex viscosity as a function of time at 37 °C.

7 h incubation, while just $16.3 \pm 2.9\%$ of the corresponding chemically activated Hep was washed out over the same time interval. Although the amount of immobilized Hep enhanced with increasing its concentration to $100 \,\mu g \, ml^{-1}$, but also led to rapid polymerization of the neutralized collagen. In this view, Hep-conjugated collagen at $50 \,\mu g \, ml^{-1}$

concentration, denoted as Col-Hep was selected for further characterizations.

The freeze-dried Col and Col-Hep matrices were characterized for their microstructure using scanning electron microscopy. As depicted in Fig. 1B–C, the Hep-Col matrix possess locally tighter microstructures likely due to Hep bound

microdomains, while the collagen fibrils are more uniformly distributed into the pristine Col matrix. In the case of Col-Hep matrix, the Hep chains bind to the amino groups of collagen through their activated carboxyl groups, which have resulted in bundled fibrils in variable arrangements.

In order to examine the effect of Hep conjugation on denaturation temperature of collagen chains, Col and Col-Hep matrices were studied by means of differential scanning calorimetry (Fig. 1D). The observed peaks are associated with the denaturation of collagen. The onset and denaturation temperatures were measured as 169.6 and 194.1 °C for Col, where shifted to higher temperatures of 205.4 and 224.8 °C for Col-Hep, respectively. The FT-IR spectra of freeze-dried Col and Col-Hep matrices are shown in Fig. 1E. In Col spectrum, a broad band associated with amine and carboxyl groups is observed around 3320 cm^{-1}. The band at 1403 cm^{-1} is associated with symmetric stretching vibrations of the carboxylate anions. As can be seen in the spectra, it is evident that Col-Hep sample show lower intensities for carboxyl and amine relevant bands in comparison with Col matrix, which corroborates conjugation of Hep chains onto the Col matrix.

Fig. 1F–H shows the evolution of the complex viscosity for Col, Col/FreeHep, and Col-Hep matrices with its absolute value $|\eta^*(\omega)|$ given by $\left|\eta^*(\omega)\right| = (G'^2 + G''^2)^{1/2}/\omega$, where G' and G'' are the storage and loss modulus, respectively. A Similar trend of G' was observed for the complex viscosity. As seen, the complex viscosity for Col-Hep is raising with time, while for Col and Col/FreeHep complex viscosity was found to decrease after reaching a maximum value. Viscoelastic properties of collagen and Col-Hep matrices were studied based on oscillatory sweep rheological measurements. Thermal evolution of the storage modulus for Col and Col-Hep solutions in the course of gelification are displayed in Fig. 2A and B, respectively. As seen, G' for both Col and Col-Hep matrices is increasing with raising temperature over the whole temperature range up to 40 °C, while decreases at temperatures beyond. G' was found to be higher for Col-Hep compared to Col matrix over the whole studied temperature range. The loss modulus for Col and Col-Hep matrices at various temperatures in the course of gelification is displayed in Fig. 2C and D, respectively. As shown, a similar trend as that of for storage modulus is observed. Fig. 2E and F displays the temperature-induced evolution of the viscoelastic damping factor (tanδ) for Col and Col-Hep matrices. According to the methodology developed by Chambon and Winter [41], the gel point is determined based on a frequency-independent value of loss tangent (tan $\delta = G''/G'$) obtained from a multi-frequency plot of tanδ versus temperature [13]. As displayed in Fig. 2E and F, the neutralized Col and Col-Hep solutions to the pH 7.4 does not show gelation behavior from a rheology point of view, but viscosification because of corresponding associations. We observed that the inclusion of activated Hep chains into the Col matrix strengthen the corresponding associations. Fig. 2E and F illustrate tanδ for Col and Col-Hep matrices is decreased with increasing temperature, which denotes gradual increase in elasticity of the matrices.

The alterations in diameter of Col and Col-Hep matrices during 3 days incubation in culture plates are displayed in Fig. 3A. The Col matrix showed considerably higher contraction compared with the Col-Hep matrix. The Col matrix was found to contract to 47.9 ± 5.8% and 34.5 ± 3.8% of its initial diameter after 12 and 72 h, while Col-Hep matrices showed markedly lower contraction. The matrix contraction results revealed that Col-Hep reaches to 76.2 ± 6.6 and 59.4 ± 6.1 of its initial diameter after 12 h and three days, respectively.

The determination of *in vitro* release profiles disclosed that the immobilization of Hep moieties into the collagen matrix have effectively retarded the release kinetics of rhBMP2 over an extended period of time of three weeks (Fig. 3B). Further, it was found that the amount of rhBMP2 washout is remarkably decreased from the Col-Hep matrix. The inset shown in Fig. 3B exhibits Col-Hep matrix significantly reduced rhBMP2 washout to 91.5 ± 27.7 ng/ml in comparison with 438.4 ± 130.3 ng/ml for the Col matrix. The viability of MC3T3 cells encapsulated in Col-Hep matrices comprising rhBMP2 was compared with the corresponding matrices in the absence of rhBMP2. The results of live/dead staining shown in Fig. 3C-F present the viability and proliferation of MC3T3 cells in the Col-Hep matrix over one week. As can be seen in Fig. 3E and F, the immobilization of rhBMP2 into the Col-Hep matrix increased the proliferation of MC3T3. It is worthy to note that the incorporated rhBMP2 into the Col matrix also provides increased MC3T3 cells proliferation though in a less pronounced manner. Alkaline Phosphatase (APase) activity, as an early osteoblastic differentiation marker [42], was investigated to evaluate the bioactivity of Col and Col-Hep matrices comprising rhBMP2. As can be seen in Fig. 3G, the Col-Hep-rhBMP2 matrix showed superior APase activity.

3.2. 3D printed βTCP based scaffolds

Tricalcium phosphate (TCP) based bioceramic scaffolds with reproducible microstructure were fabricated using the additive layer manufacturing technique. The microstructure of the scaffolds was shown in Fig. 4 A, B. The measured mean ± Standard deviation of pore size of the scaffolds was 497 ± 18 μm and 416 ± 23 μm before and after sintering, respectively. The strand thickness was 514 ± 7 μm, and the porosity of scaffolds was 47.5 ± 3.4%. The compressive strength of β-TCP based scaffolds was measured to be 10.82 ± 4.6 MPa. The compressive modulus for the scaffolds was measured to be 85.9 ± 4.8 MPa.

3.3. Cell seeding strategies

The seeding efficacy of MSCs through the gels was 100%, however by directly seeding the MSCs on the 3D printed scaffolds, the 21.75% of MSCs was attached to the scaffolds. The viability of MSc seeded directly on the 3D printed β-TCP scaffold was compared to MSCs laden constructs over two weeks. The results demonstrate significantly improved proliferation of MSCs loaded into the gels and seeded on the constructs compared with MSCs directly seeded on the β-TCP scaffold. The ALP expression of MSCs loaded into the gels and seeded on 3D scaffolds was found to be significantly higher than the other group.
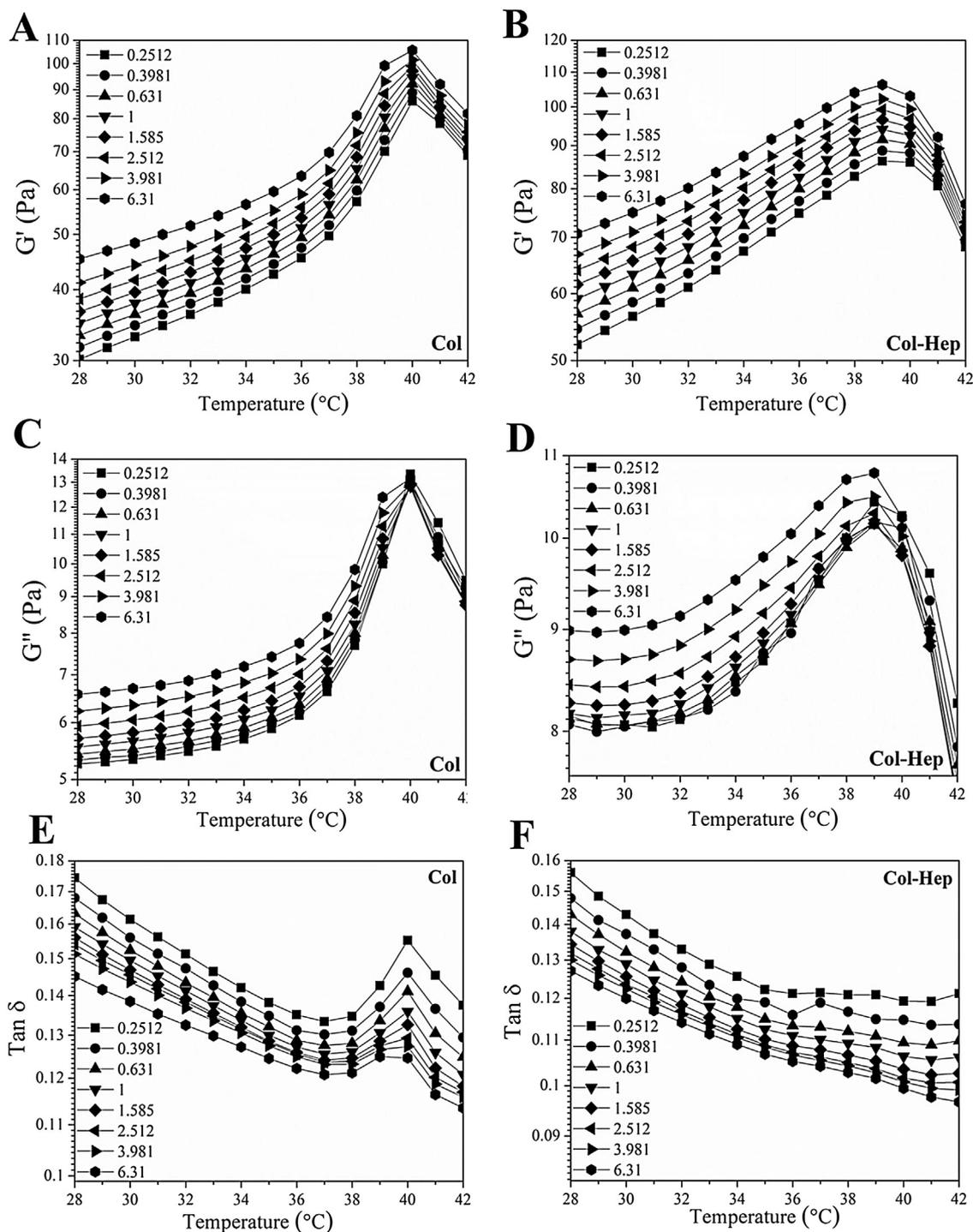
Fig. 2 – Rheological characterization of Col and Col-Hep matrices: storage modulus (G′) as a function of temperature at the indicated frequencies for (A) Col, and (B) Col-Hep matrices. Thermal evolution of the loss modulus (G″) for (C) Col, and (D) Col-Hep matrices. Temperature-induced evolution of the viscoelastic loss tangent (tanδ) for (E) Col, and (F) Col-Hep matrices.

3.4. 3D Printed reinforced Col-Hep matrix

The SEM micrographs of Col-Hep and Col-Hep-rhBMP2 matrices encapsulating MSCs, which were supported by the 3D printed β-TCP scaffolds are shown in Fig. 4C, D. As seen, the Fig. 5E, reinforced Col-Hep-rhBMP2 matrix shows improved proliferation of 3D cultured MSCs. The DNA PicoGreen assay

was used to assess the combinatorial effects the triad key elements of scaffold, cells and the growth factor in Col/β-TCP, Col-Hep/β-TCP and Col-Hep-rhBMP2/β-TCP constructs. MSCs proliferated in all three groups up to 21 days. Further, it was found that the proliferation rate of MSCs was significantly higher in Col-Hep-rhBMP2/β-TCP constructs compared to Col/β-TCP and Col-Hep/β-TCP after 3, 7, 14 and 21 days
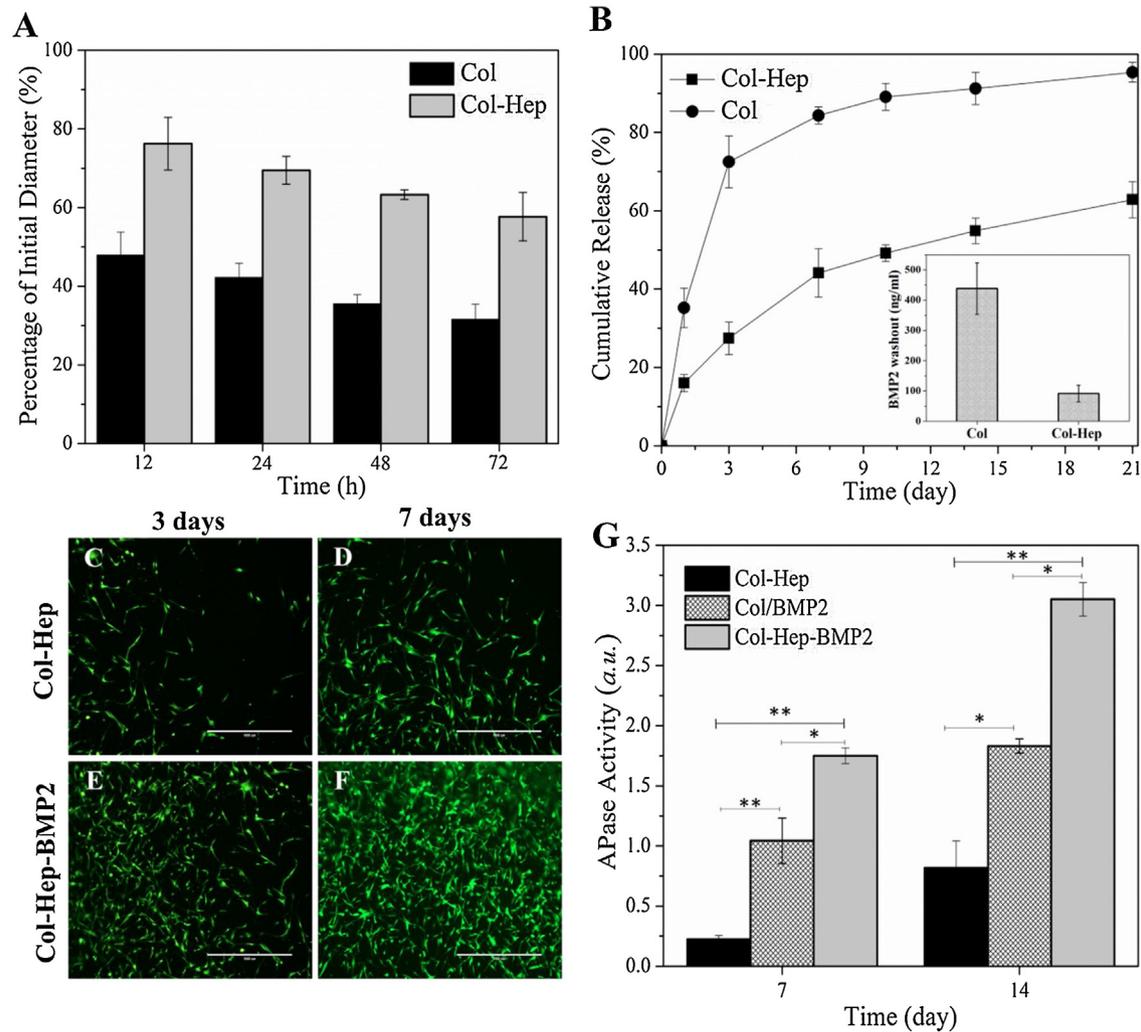
Fig. 3 – (A) Matrix contraction for Col and Col-Hep matrices over three days. (B) The release pattern of rhBMP2 from Col and Col-Hep matrices over three weeks (The inset shows the rhBMP2 washout from Col and Col-Hep matrices after 4 h). Viability of MC3T3 encapsulated in Col-Hep matrix after (C) 3 days, and (D) 7 days. Viability of MC3T3 encapsulated in Col-Hep matrix comprising rhBMP2 after (E) 3 days, and (F) 7 days. (G) APase activity of 3D cultured MC3T3 in Col-Hep, Col/rhBMP2, and Col-Hep-rhBMP2 matrices.

(P < 0.01). However, Col-Hep/β-TCP showed a similar proliferation rate of encapsulated MSCs to Col/β-TCP over three weeks. Fig. 5F shows the APase activity of Col/β-TCP, Col-Hep/β-TCP and Col-Hep-rhBMP2/β-TCP constructs to examine the effects of combined scaffold, cells and growth factors. The highest APase activity was observed for the Col-Hep-rhBMP2/β-TCP (P < 0.01). The APase activity of cells was found to increase for 21 days in all three groups. Col-Hep-rhBMP2/β-TCP construct showed significant greater cells proliferation rate and APase activity compared to Col/β-TCP, Col-Hep/β-TCP constructs after 3, 7, 14 and 21 days. Fig. 5 A–D, shows the immunofluorescent images of osteocalcin marker for encapsulated MSCs into Col-Hep and Col-Hep-rhBMP2 matrices supported by the 3D printed β-TCP scaffolds after 14 and 21 days. The images demonstrate that OCN marker is higher in the presence of rhBMP2 after 14 and 21 days. Quantitative real-time PCR analysis for RUNX-2, OCN and ALP of MSCs cultured on β-TCP/Col-Hep and β-TCP/Col-Hep-rhBMP2 construct

are presented in Fig. 5G–H. The qPCR analysis showed that the mRNA expressions of RUNX-2, OCN and ALP were significantly higher in the immobilized rhBMP2 group after 7 and 14 days (P < 0.01). The expressions of RUNX-2, OCN and ALP were upregulated 1.2 fold, 2.4 and 2.3 fold at day 14 (P < 0.01), respectively.

3.5. Subcutaneous implantation of constructs

Regeneration was uneventful in all of the subcutaneous surgical sites. Neither severe inflammation nor foreign body reaction was seen in any of the tissue evaluated (Fig. 6). In all constructs, the newly created tissue varied in size, comprising of thin pieces of mineralized tissue and large marrow spaces with connective tissue cells and occasional hematopoietic cells. Cuboidal osteoblast-like cells were found to be regenerating the constructs to varying degrees along the mineralized tissue in all of the groups. More obvious findings of miner-
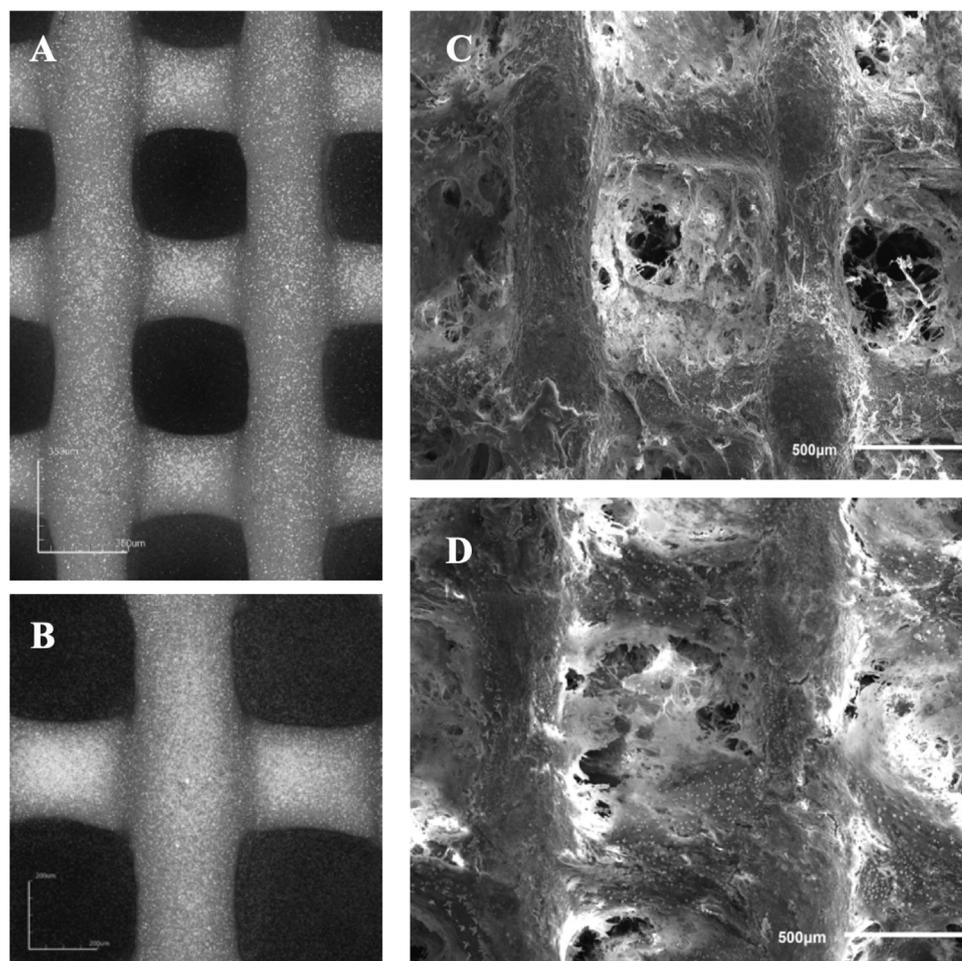
Fig. 4 – 3D laser scanning micrographs of the 3D-printed β-TCP scaffold (A, B), Scanning electron micrographs of (C), Col-Hep and (D), Col-Hep-rhBMP2 matrices encapsulating MSCs filled into the 3D printed β-TCP scaffolds after 21 days (A, B: scale bar is 500 μm).

alized tissue were often found in the βTCP/Col-BMP2 + MSCs and βTCP/Col-Hep BMP2+ MSCs scaffolds. Furthermore, direct bone-biomaterial contact and new bone formation occurred to a greater degree in the βTCP/Col-Hep BMP2 + MSCs group. The RNA expression level of osteogenic related genes including RUNXII, OCN, and ALP, were evaluated by qPCR and showed significant differences between the BMP2 containing groups, βTCP/Col-BMP2 + MSCs and βTCP/Col-Hep BMP2 + MSCs, and control group without BMP2, βTCP/Col-Hep + MSCs, and also between immobilized BMP2, βTCP/Col-Hep BMP2+ MSCs, and loaded BMP2 scaffold groups. Addition of BMP2 in the form of immobilization leads to a significant increase in RNA expression toward osteogenesis.

4. Discussion

Critical-sized bone defects typically fail to regenerate spontaneously through endogenous healing process [1]. Stem cell-based bone tissue engineering strategies are very promising approach aims to regenerate critical size defects through integrating a triad of elements: scaffolds, growth factors, and stem/progenitor cells [20,43,44]. Many conventional approaches, including implantation of MSCs loaded on prefabricated scaffolds or developing of injectable growth factors delivery systems, have been explored to address clinical challenges [45–47]. However, there are still challenges in design of an ideal scaffold as the cell delivery vehicle with controlled release of growth factors with proper anatomical geometries and physical properties to engineer new bone tissue [10,48,49]. Researchers are investigating different approaches to utilize stem cells for bone tissue regeneration; however, in order to harness the full potential of stem cell therapy, the scaffold should retain stem cells at the target site after implantation as well as preserve the critical characteristics of stem cells such as self-renewal and support them to differentiate [10,50,51].

In this article, a combinatorial approach consisting synthesis of a BMP2 immobilized collagen-heparin matrix supported by a 3D printed bioactive ceramic scaffold was proposed to efficiently deliver MSCs. In the proposed methodology, collagen 3D matrix was functionalized with heparin to immobilize rhBMP2 to offer a 3D microenvironment for harnessing osteogenic capacity of MSCs. Furthermore, the supportive bioceramic scaffold play the essential roles of reinforcing and forming the biomimetic gel into desired scaffold constructs.
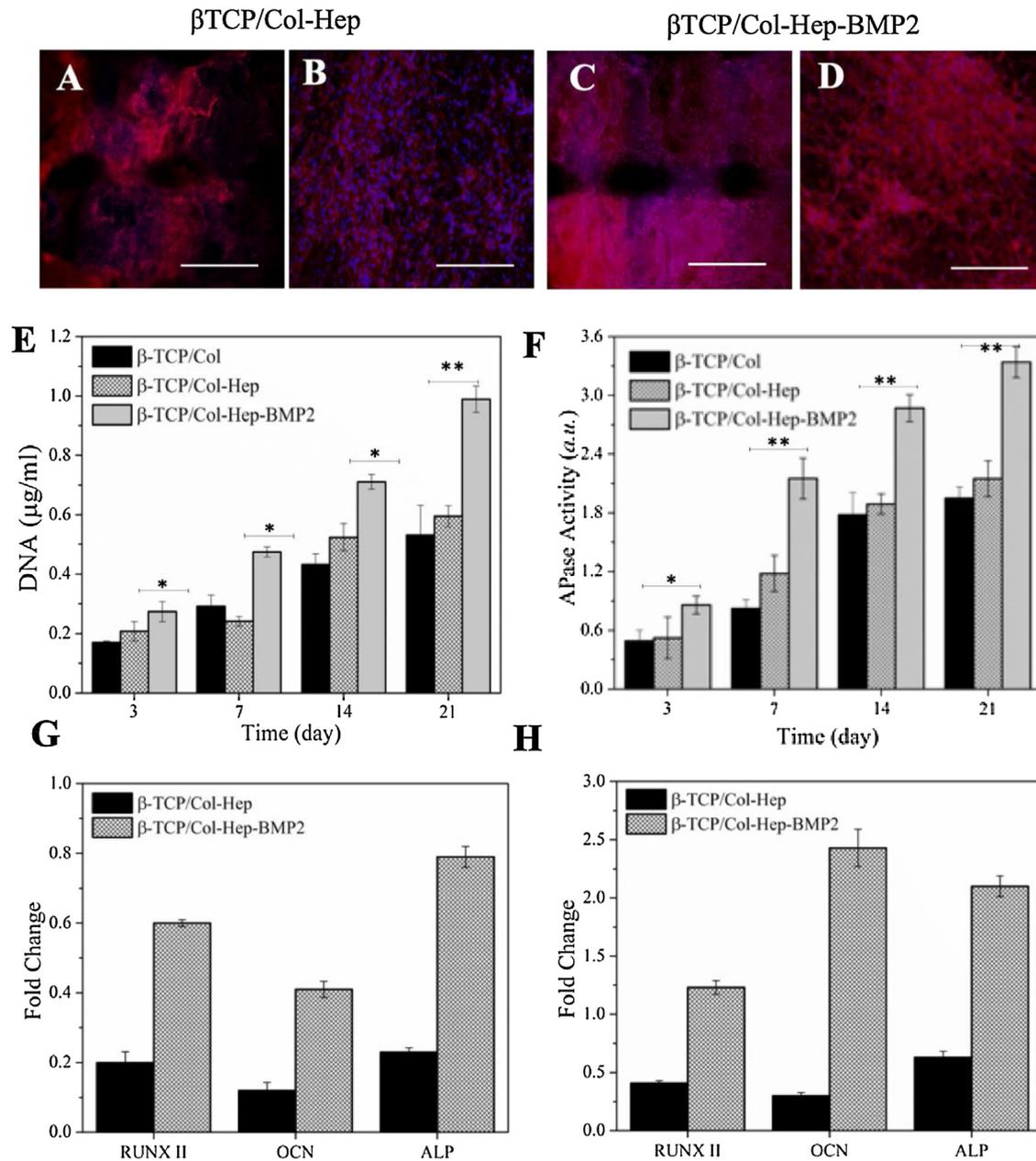
Fig. 5 – (A-D) The immunofluorescent images of osteocalcin marker for encapsulated MSCs into β-TCP/Col-Hep and β-TCP/Col-Hep-rhBMP2 matrices scaffolds after 21 days scale bar is 500 μm). (A-B) for β-TCP/Col-Hep, and (C-D) for β-TCP/Col-Hep-rhBMP2. (E) DNA quantification of MSCs cultured β-TCP/Col, β-TCP/Col-Hep and β-TCP/Col-Hep-rhBMP2 constructs. (F) Alkaline phosphatase (APase) activity of MSCs cultured β-TCP/Col, β-TCP/Col-Hep and β-TCP/Col-Hep-rhBMP2 constructs. Quantitative real-time PCR analysis for RUNX-2, OCN and ALP of MSCs cultured β-TCP/Col-Hep and β-TCP/Col-Hep-rhBMP2 constructs after 7 days (G) and 14 days (H).

Additive manufacturing techniques offer customized scaffold fabrication from a computer aided design for patient-specific defects. 3D printing offers great control over scaffold microstructure, minimal contamination from added material, and direct fabrication of ceramic biomaterials with high geometric complexity [4,5]. However, this approach like conventional prefabricated scaffolds suffers from relatively low cell seeding efficiency and cell retention with cell seeding-depth limitations [52]. Herein we designed a bone ECM-mimetic 3D gel matrix to *in situ* seed and be mechani-

cally supported by a 3D printed reinforced porous bioceramic scaffold. In other words, in order to tackle seeding-depth limitations and cell retention the collagen hydrogel with encapsulated MSCs were injected into the predesigned scaffolds.

The *in vitro* and *in vivo* results detailed in this article showed the successful combination of the benefits of heparin functionalized collagen to deliver the MSCs and immobilized the BMP2. The collagen type I is the main constituent of natural bone ECM; however, reconstituted collagen matrix has a low
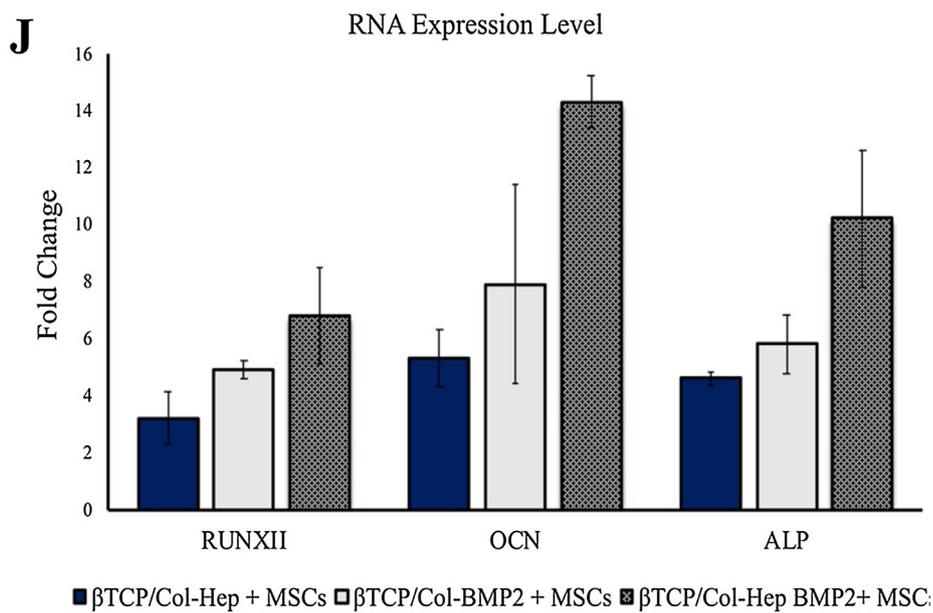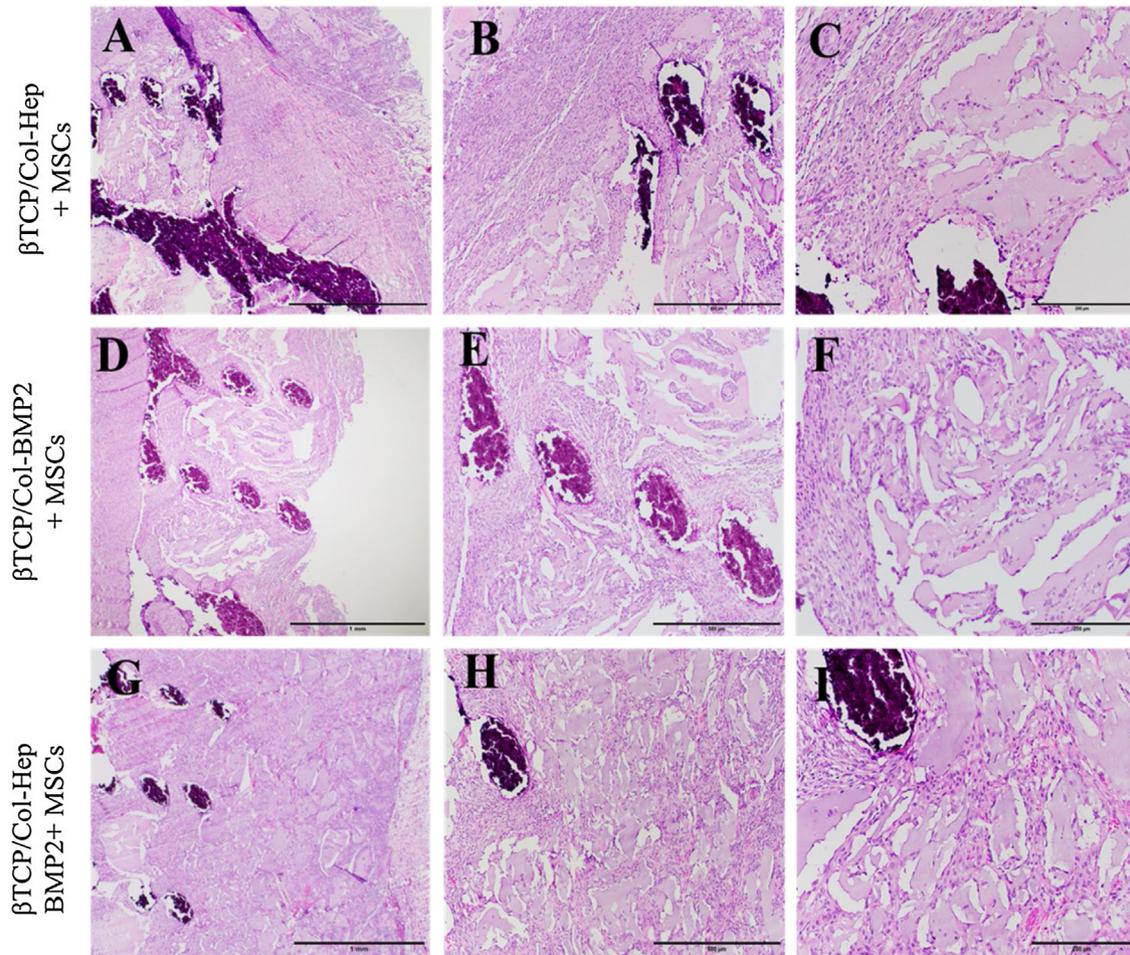
Fig. 6 – Hematoxylin and eosin staining of sections from decalcified scaffolds loaded with cells (A–C), βTCP/Col-Hep + MSCs (D–F), βTCP/Col-BMP2 + MSCs and (G–I), βTCP/Col-Hep BMP2+ MSCs scaffolds after 6 weeks of subcutaneous implantation (J) Quantitative real-time PCR analysis for RUNX-2, OCN and ALP of MSCs cultured β-TCP/Col-Hep and β-TCP/Col-Hep-rhBMP2 constructs after 6 weeks of subcutaneous implantation.

mechanical property and shows relatively high gel contraction. To overcome contraction shortcoming of collagen gel and provide the availability of BMP2, the collagen matrix was modified through chemical functionalization with heparin (Hep) to immobilize rhBMP2. In order to achieve efficient binding domains into the collagen matrix, the carboxyl groups of Hep was activated *via* carbodiimide chemistry prior to reaction with collagen chains. It was demonstrated that the chemical functionalization of activated Hep onto collagen chains prior to polymerization provides proper localization of the GAG moieties for efficient immobilization of rhBMP2. Further, we found that such an ECM-mimetic approach also offers significantly reduced contraction of collagen matrix, while improving its viscoelastic features. Col matrix is composed of evenly distributed fibrils, whereas fibrillar associations were found to become locally interlocked after inclusion of heparin into the Col-Hep matrix. Besides covalent bonds, the structural stability of Hep in collagen matrix depends on other interactions including electrostatic, hydrophobic, and hydrogen bonds contributing to the integrity of collagen suprastructure. As discussed below, these interactions reduce the collagen matrix contraction, which is vital to provide a robust 3D culture microenvironment for the encapsulated cells.

The significantly lower contraction of Col-Hep compared to the Col matrices originates from the associations developed into the Col fibrillar network through incorporated Hep chains with active carboxyl moieties (refer to discussions related to improved viscoelastic features of Col matrix after inclusion of Hep chains). The mechanisms behind lower contraction of cell-laden Col-Hep matrices can be described based on the changes in collagen fibril polymerization and organization in the presence of heparin. In the course of Col matrix gelification, the collagen fibrils gradually surround the cells. During such process, one or more collagen chains can bond to the cell surface, followed by their reorganization in microdomains adjacent to the cells. Such molecular reorganizations in the vicinity of cells occur through cytoskeleton-dependent rearrangement of actin filaments [56]. Subsequently, intermolecular associations among collagen fibrils are stabilized through intra- and intermolecular noncovalent interactions along with Col-Hep covalent bindings. It can be inferred that such interlocked microdomains have preserved the integrity of the Col-Hep matrix over time against cellular mechanical forces and enzymatic activities. These findings resemble the remarkable amount of heparin found in fibrous tissues and scars, which has been understood to interrupt the ability of fibroblasts to remodel the synthesized collagenous matrix [57].

Thermal denaturation of collagen fibrils take place due to molecular conformational changes triggered by cleavage of intermolecular bonds including glycosylation of lysine, hydroxylysine residues and disulfide bonds [53]. Hence, the postponed denaturation onset and peak temperatures for Col-Hep matrix implies that the Hep conjugation has hindered fragmentation of the collagen chains through formation of crosslinks which stabilize the fibrillar ultrastructure [54].

The rheological properties of Col-Hep matrices were also studied to find the effect of Hep to direct the intermolecular crosslinks among collagen chains. It should be noted that the relative higher elasticity of the Col matrix after inclusion of FreeHep relies on the possible interactions among Hep and collagen chains including electrostatic, hydrophobic and hydrogen bonds. The Col-Hep matrix showed significantly improved elasticity. This finding confirms an important role for Hep chains with activated carboxyl groups to chemically bond into collagen chains and form bridges among fibrillar structures to strengthen the Col-Hep network. It is worth to note that such covalent bonds are also responsible for the stabilization of the Col-Hep matrix beyond gelification, and eliminate the syneresis effect as well. Such interactions in Col-Hep result in considerably reduced matrix contraction. The sharp increase in complex viscosity for Col-Hep matrix is associated with collagen fibril formation along with intermolecular conjugation of Hep chains. In other words, multi-site covalent bonds among collagen and preactivated Hep chains play a predominant role in the Col-Hep matrix strength.

The higher elasticity of Col-Hep compared with Col matrix originates from intermolecular crosslinking among Hep comprising activated carboxyl moieties with amine groups on collagen chains. In contrast to Col-Hep matrix which showed increasing network elasticity over time, the observed decrease in complex viscosity and elasticity of Col and Col/FreeHep matrices after an initial increase could be attributed to the syneresis effect. Furthermore, the drop-in elasticity of the networks at elevated temperature range is due to conformational change of collagen chains along with screening of the hydrogen bonded water molecules stabilizing them. It should be noted that although activated Hep chains have effectively contributed to an increase in elasticity of the Col matrix, they could not postpone disintegration of the network. Accordingly, it is inferred that the Hep chains are locally conjugated to the collagen fibrillar network and are not percolated due to limited incorporated Hep content ($50\,mg\,ml^{-1}$), which was intended to prohibit macro phase separation while maintaining proper handling of the Col-based matrix.

To study the gelation behavior, the temperature sweeps multi-frequency plot of damping factor for the neutralized Col and Col-Hep solutions does not show gelation behavior. Indeed, the observed gelification for such systems is due to the temperature induced association of self-assembled collagen chains into fibrillar structures. At the physiological pH (7.4) and temperature (37 °C), collagen chains undergo axial alignment and connectivity among neighboring collagen triple helices is established [55]. The damping factor was found to be lower for Col-Hep in comparison with Col matrix in the course of temperature triggered gelification process. This implies interfibrillar connectivity and percolation of the collagen fibrils which have been facilitated in the presence of Hep chains.

Several animal and clinical studies have confirmed that delivery of MSCs embedded in scaffolds in the presence of osteoinductive growth factors results in higher bone healing compared to cell delivery alone. Bone morphogenic proteins (BMPs) are the most osteoinductive growth factors; however, their clinical administration has been limited by their short half-life, rapid distribution by body fluids and large doses required [24,27]. Although BMP2 delivery using various carrier systems especially polymeric materials has been shown in several pre-clinical and clinical studies, it is still challenging to succeed a controlled introduction of BMP2 while preserving its bioactivity and reducing the applied quantity

of growth factors. Therefore, in this study we intended to develop a bone-engineered hybrid constructs with consistent osteogenic ability to accommodate MSCs with the capability of providing spatiotemporal bioavailability of rhBMP2.

Considering the rapid release of biomacromolecules including growth factors from gel-like matrices [56,57], we have synthesized a collagen based matrix modified with heparin moieties to achieve sustained release of rhBMP2. In fact, the conjugation of Hep moieties enhances the affinity of Col matrix to achieve enhanced controlled release of rhBMP2. The electrostatic interactions between positively charged amino groups of rhBMP2 and negatively charged sulfate groups in heparin, in addition to the strong binding of the N-terminal segments in BMP2 to heparin provides its retention and sustained release [26]. Heparin chains are known to possess higher negative charge density compared to other biomacromolecules comprising sulfate and carboxyl groups [58]. Further, it has been found that in the presence of heparin, degradation of rhBMP2 can be inhibited by reducing interaction with its noggin [59]. Thus, the rhBMP2 activity is prolonged in the presence of heparin. Consistent with our study, Lin et al. showed BMP2 immobilized in heparin-crosslinked demineralized bone matrix increase the APase activity and calcification [60].

The binding of BMP-2 to its receptors on MSCs is of high fundamental and clinical interest. which provokes the MSCs differentiation into osteoblasts [61]. Our alkaline phosphatase and qPCR results obtained after *in vitro* culturing of the MSCs and subcutaneous implantation of the scaffolds showed that the addition of BMP2 specially in the form of immobilization leads to a significant increase in RNA expression toward osteogenesis. The qPCR assessment was used to analyze the gene expression levels of terminal osteogenesis related markers. The qPCR analysis showed that the mRNA expression of RUNX-2, OCN and ALP were significantly higher in the immobilized rhBMP2 group after 7 and 14 days. Our results are consisting with other published article on positive effects of BMP2 immobilization. In rat ectopic model, Chen et al. [62] showed that treatment with immobilized BMP2 resulted in upregulation of osteogenic markers including Runx2 OPN and ALP. Our results on *in vitro* and *in vivo* characterization of Col-Hep-rhBMP2 matrices encapsulating MSCs supported by 3D printed β-TCP scaffolds suggest that the implemented methodology provide promising integration of growth factors and stem cells toward personalized engineering of bone tissue.

5. Conclusion

Current study presents a combinatorial bone tissue engineering strategy to develop an ECM-mimetic 3D gel to enhance the seeding efficiency and osteogenesis activity of MSCs trough 3D printed scaffolds. The developed constructs were consisted of heparin conjugated collagen hydrogel immobilizing BMP2, which was reinforced by 3D printed β-TCP-based bioceramic scaffold. Rheological characterizations of heparin-conjugated collagen gel revealed their improved elasticity while suppressing the matrix contraction over time. The obtained results revealed the great capability of heparin functionalized collagen to retain the bioactivity of growth factors and support

MSCs viability and differentiation toward bone regeneration. The *in vivo* histology and real-time polymerase chain reaction (qPCR) analysis showed that the designed construct supported the osteogenic differentiation of MSCs and induced the ectopic bone formation in the rat model. It is worth to note that the proposed methodology can be established to integrate other osteogenic cells and growth factors for patient-specific regenerative medicine applications.

Appendix A. Supplementary data

Supplementary material related to this article can be found, in the online version, at doi:https://doi.org/10.1016/j.dental.2019.04.004.

REFERENCES

[1] Zhang X, Li Y, Chen YE, Chen J, Ma PX. Cell-free 3D scaffold with two-stage delivery of miRNA-26a to regenerate critical-sized bone defects. Nat Commun 2016;7:10376.

[2] Bauer TW, Muschler GF. Bone graft materials: an overview of the basic science. Clin Orthop Relat Res 2000;371:10–27.

[3] Raftery RM, Mencía-Castaño I, Sperger S, Chen G, Cavanagh B, Feichtinger GA, et al. Delivery of the improved BMP-2-Advanced plasmid DNA within a gene-activated scaffold accelerates mesenchymal stem cell osteogenesis and critical size defect repair. J Control Release 2018;283:20–31.

[4] Fahimipour F, Dashtimoghadam E, Rasoulianboroujeni M, Yazdimamaghani M, Khoshroo K, Tahriri M, et al. Collagenous matrix supported by a 3D-printed scaffold for osteogenic differentiation of dental pulp cells. Dent Mater 2018;34:209–20.

[5] Fahimipour F, Rasoulianboroujeni M, Dashtimoghadam E, Khoshroo K, Tahriri M, Bastami F, et al. 3D printed TCP-based scaffold incorporating VEGF-loaded PLGA microspheres for craniofacial tissue engineering. Dent Mater 2017;33:1205–16.

[6] Inzana JA, Olvera D, Fuller SM, Kelly JP, Graeve OA, Schwarz EM, et al. 3D printing of composite calcium phosphate and collagen scaffolds for bone regeneration. Biomaterials 2014;35:4026–34.

[7] Pati F, Song T-H, Rijal G, Jang J, Kim SW, Cho D-W. Ornamenting 3D printed scaffolds with cell-laid extracellular matrix for bone tissue regeneration. Biomaterials 2015;37:230–41.

[8] Vallet-Regí M, Ruiz-Hernández E. Bioceramics: from bone regeneration to cancer nanomedicine. Adv Mater 2011;23:5177–218.

[9] Shao Y, Fu J. Integrated micro/nanoengineered functional biomaterials for cell mechanics and mechanobiology: a materials perspective. Adv Mater 2014;26:1494–533.

[10] Whitely M, Cereceres S, Dhavalikar P, Salhadar K, Wilems T, Smith B, et al. Improved in situ seeding of 3D printed scaffolds using cell-releasing hydrogels. Biomaterials 2018;185:194–204.

[11] Seliktar D. Designing cell-compatible hydrogels for biomedical applications. Science 2012;336:1124–8.

[12] Prince E, Kumacheva E. Design and applications of man-made biomimetic fibrillar hydrogels. Nat Rev Mater 2019:1.

[13] Dashtimoghadam E, Bahlakeh G, Salimi-Kenari H, Hasani-Sadrabadi MM, Mirzadeh H, Nyström B. Rheological study and molecular dynamics simulation of biopolymer blend thermogels of tunable strength. Biomacromolecules 2016;17:3474–84.

[14] Dashtimoghadam E, Mirzadeh H, Taromi FA, Nyström B. Thermoresponsive biopolymer hydrogels with tunable gel characteristics. RSC Adv 2014;4:39386–93.

[15] Huebsch N, Arany PR, Mao AS, Shvartsman D, Ali OA, Bencherif SA, et al. Harnessing traction-mediated manipulation of the cell/matrix interface to control stem-cell fate. Nat Mater 2010;9:518.

[16] Chaudhuri O, Gu L, Klumpers D, Darnell M, Bencherif SA, Weaver JC, et al. Hydrogels with tunable stress relaxation regulate stem cell fate and activity. Nat Mater 2016;15:326.

[17] Zhang Y, Zhu D, Wei Y, Wu Y, Cui W, Liuqin L, et al. A collagen hydrogel loaded with HDAC7-derived peptide promotes the regeneration of infarcted myocardium with functional improvement in a rodent model. Acta Biomater 2019.

[18] Chan BP, Hui T, Yeung C, Li J, Mo I, Chan G. Self-assembled collagen–human mesenchymal stem cell microspheres for regenerative medicine. Biomaterials 2007;28:4652–66.

[19] Ferreira AM, Gentile P, Chiono V, Ciardelli G. Collagen for bone tissue regeneration. Acta Biomater 2012;8:3191–200.

[20] Khojasteh A, Fahimipour F, Jafarian M, Sharifi D, Jahangir S, Khayyatan F, et al. Bone engineering in dog mandible: coculturing mesenchymal stem cells with endothelial progenitor cells in a composite scaffold containing vascular endothelial growth factor. J Biomed Mater Res B Appl Biomater 2017;105:1767–77.

[21] Ingavle GC, Gionet-Gonzales M, Vorwald CE, Bohannon LK, Clark K, Galuppo LD, et al. Injectable mineralized microsphere-loaded composite hydrogels for bone repair in a sheep bone defect model. Biomaterials 2019;197:119–28.

[22] Buduru S, Gulei D, Zimta A-A, Tigu A, Cenariu D, Berindan-Neagoe I. The potential of different origin stem cells in modulating oral bone regeneration processes. Cells 2019;8:29.

[23] Cao L, Wang J, Hou J, Xing W, Liu C. Vascularization and bone regeneration in a critical sized defect using 2-N, 6-O-sulfated chitosan nanoparticles incorporating BMP-2. Biomaterials 2014;35:684–98.

[24] Migliorini E, Valat A, Picart C, Cavalcanti-Adam EA. Tuning cellular responses to BMP-2 with material surfaces. Cytokine Growth Factor Rev 2016;27:43–54.

[25] Nohe A, Hassel S, Ehrlich M, Neubauer F, Sebald W, Henis YI, et al. The mode of bone morphogenetic protein (BMP) receptor oligomerization determines different BMP-2 signaling pathways. J Biol Chem 2002;277:5330–8.

[26] Ruppert R, Hoffmann E, Sebald W. Human bone morphogenetic protein 2 contains a heparin-binding site which modifies its biological activity. Eur J Biochem 1996;237:295–302.

[27] Kim M, Choe S. BMPs and their clinical potentials. BMB Rep 2011;44:619.

[28] Geiger M, Li R, Friess W. Collagen sponges for bone regeneration with rhBMP-2. Adv Drug Deliv Rev 2003;55:1613–29.

[29] Lee K, Silva EA, Mooney DJ. Growth factor delivery-based tissue engineering: general approaches and a review of recent developments. J R Soc Interface 2011;8:153–70.

[30] Ruoslahti E, Yamaguchi Y. Proteoglycans as modulators of growth factor activities. Cell 1991;64:867–9.

[31] Anjum F, Lienemann PS, Metzger S, Biernaskie J, Kallos MS, Ehrbar M. Enzyme responsive GAG-based natural-synthetic hybrid hydrogel for tunable growth factor delivery and stem cell differentiation. Biomaterials 2016;87:104–17.

[32] Freudenberg U, Liang Y, Kiick KL, Werner C. Glycosaminoglycan-based biohybrid hydrogels: a sweet and smart choice for multifunctional biomaterials. Adv Mater 2016.

[33] Bhakta G, Rai B, Lim ZX, Hui JH, Stein GS, van Wijnen AJ, et al. Hyaluronic acid-based hydrogels functionalized with heparin that support controlled release of bioactive BMP-2. Biomaterials 2012;33:6113–22.

[34] Hettiaratchi MH, Miller T, Temenoff JS, Guldberg RE, McDevitt TC. Heparin microparticle effects on presentation and bioactivity of bone morphogenetic protein-2. Biomaterials 2014;35:7228–38.

[35] Hou Y-T, Ijima H, Takei T, Kawakami K. Growth factor/heparin-immobilized collagen gel system enhances viability of transplanted hepatocytes and induces angiogenesis. J Biosci Bioeng 2011;112:265–72.

[36] Wissink M, Beernink R, Pieper J, Poot A, Engbers G, Beugeling T, et al. Immobilization of heparin to EDC/NHS-crosslinked collagen. Characterization and in vitro evaluation. Biomaterials 2001;22:151–63.

[37] Mahmoudi T, Karimkhani V, Song GS, Lee DS, Stadler FJ. Shear induced irreversible gelation through physical network formation. Macromolecules 2013;46:4141–50.

[38] Ngo P, Ramalingam P, Phillips JA, Furuta GT. Collagen gel contraction assay. Cell-cell interactions. Springer; 2006. p. 103–9.

[39] Wiemann M, Rumpf H, Bingmann D, Jennissen H. The binding of rhBMP-2 to the receptors of viable MC3T3-E1 cells and the question of cooperativity. Materialwissenschaft und Werkstofftechnik: Mater Sci Eng Technol 2001;32:931–6.

[40] Sobral JM, Caridade SG, Sousa RA, Mano JF, Reis RL. Three-dimensional plotted scaffolds with controlled pore size gradients: effect of scaffold geometry on mechanical performance and cell seeding efficiency. Acta Biomater 2011;7:1009–18.

[41] Chambon F, Winter HH. Linear viscoelasticity at the gel point of a crosslinking PDMS with imbalanced stoichiometry. J Rheol 1987;31:683–97.

[42] Rimando MG, Wu H-H, Liu Y-A, Lee C-W, Kuo S-W, Lo Y-P, et al. Glucocorticoid receptor and histone deacetylase 6 mediate the differential effect of dexamethasone during osteogenesis of mesenchymal stromal cells (MSCs). Sci Rep 2016;6.

[43] Lee K, Chan CK, Patil N, Goodman SB. Cell therapy for bone regeneration—bench to bedside. J Biomed Mater Res B: Appl Biomater 2009;89:252–63.

[44] Nuñez J, Vignoletti F, Caffesse RG, Sanz M. Cellular therapy in periodontal regeneration. Periodontol 2000 2019;79:107–16.

[45] Taba Jr M, Jin Q, Sugai J, Giannobile W. Current concepts in periodontal bioengineering. Orthod Craniofac Res 2005;8:292–302.

[46] De Witte T-M, Fratila-Apachitei LE, Zadpoor AA, Peppas NA. Bone tissue engineering via growth factor delivery: from scaffolds to complex matrices. Regen Biomater 2018;5:197–211.

[47] Khojasteh A, Fahimipour F, Eslaminejad MB, Jafarian M, Jahangir S, Bastami F, et al. Development of PLGA-coated β-TCP scaffolds containing VEGF for bone tissue engineering. Mater Sci Eng C 2016;69:780–8.

[48] Dang M, Saunders L, Niu X, Fan Y, Ma PX. Biomimetic delivery of signals for bone tissue engineering. Bone Res 2018;6.

[49] Marquardt LM, Heilshorn SC. Design of injectable materials to improve stem cell transplantation. Curr Stem Cell Rep 2016;2:207–20.

[50] Burdick JA, Mauck RL, Gerecht S. To serve and protect: hydrogels to improve stem cell-based therapies. Cell Stem Cell 2016;18:13–5.

[51] Sears N, Dhavalikar P, Whitely M, Cosgriff-Hernandez E. Fabrication of biomimetic bone grafts with multi-material 3D printing. Biofabrication 2017;9:025020.

[52] Cohen DL, Malone E, Lipson H, Bonassar LJ. Direct freeform fabrication of seeded hydrogels in arbitrary geometries. Tissue Eng 2006;12:1325–35.

[53] Miles CA, Bailey AJ. Thermal denaturation of collagen revisited. J Chem Sci 1999;111:71–80.

[54] Robins SP, Bailey AJ. The chemistry of the collagen cross-links. The mechanism of stabilization of the reducible intermediate cross-links. Biochem J 1975;149:381–5.

[55] Rosenblatt J, Devereux B, Wallace D. Injectable collagen as a pH-sensitive hydrogel. Biomaterials 1994;15:985–95.

[56] Hoare TR, Kohane DS. Hydrogels in drug delivery: progress and challenges. Polymer 2008;49:1993–2007.

[57] Wallace DG, Rosenblatt J. Collagen gel systems for sustained delivery and tissue engineering. Adv Drug Deliv Rev 2003;55:1631–49.

[58] Bramono DS, Murali S, Rai B, Ling L, Poh WT, Lim ZX, et al. Bone marrow-derived heparan sulfate potentiates the osteogenic activity of bone morphogenetic protein-2 (BMP-2). Bone 2012;50:954–64.

[59] Zhao B, Katagiri T, Toyoda H, Takada T, Yanai T, Fukuda T, et al. Heparin potentiates the in vivo ectopic bone formation induced by bone morphogenetic protein-2. J Biol Chem 2006;281:23246–53.

[60] Lin H, Zhao Y, Sun W, Chen B, Zhang J, Zhao W, et al. The effect of crosslinking heparin to demineralized bone matrix on mechanical strength and specific binding to human bone morphogenetic protein-2. Biomaterials 2008;29:1189–97.

[61] Scarfì S. Use of bone morphogenetic proteins in mesenchymal stem cell stimulation of cartilage and bone repair. World J Stem Cells 2016;8:1.

[62] Chen Z, Zhang Z, Feng J, Guo Y, Yu Y, Cui J, et al. Influence of Mussel-Derived Bioactive BMP-2-Decorated PLA on MSC Behavior in Vitro and Verification with Osteogenicity at Ectopic Sites in Vivo. ACS Appl Mater Interfaces 2018;10:11961–71.